Adiabatic Expansion of Electron Gas in a Magnetic Nozzle

Kazunori Takahashi,[1,*] Christine Charles,[2] Rod Boswell,[2] and Akira Ando[1]
[1]Department of Electrical Engineering, Tohoku University, Sendai 980-8579, Japan
[2]Space Plasma, Power and Propulsion Laboratory, Research School of Physics and Engineering, The Australian National University, Canberra, Australian Capital Territory 2601, Australia

(Received 16 October 2017; revised manuscript received 8 December 2017; published 26 January 2018)

A specially constructed experiment shows the near perfect adiabatic expansion of an ideal electron gas resulting in a polytropic index greater than 1.4, approaching the adiabatic value of 5/3, when removing electric fields from the system, while the polytropic index close to unity is observed when the electrons are trapped by the electric fields. The measurements were made on collisionless electrons in an argon plasma expanding in a magnetic nozzle. The collision lengths of all electron collision processes are greater than the scale length of the expansion, meaning the system cannot be in thermodynamic equilibrium, yet thermodynamic concepts can be used, with caution, in explaining the results. In particular, a Lorentz force, created by inhomogeneities in the radial plasma density, does work on the expanding magnetic field, reducing the internal energy of the electron gas that behaves as an adiabatically expanding ideal gas.

DOI: 10.1103/PhysRevLett.120.045001

The first law of thermodynamics is that the change in the internal energy of a closed system (ΔU) is equal to the added heat (Q) minus the net work (W) done by the system: $\Delta U = Q + W$, and for an expanding system, W can be calculated by the pressure P and the change in volume ΔV as $\Delta U = Q - P\Delta V$. These changes are identified using a calorimeter; for plasmas, a detailed energy distribution of the charged particles can be obtained using a Langmuir probe [1].

Isothermal and adiabatic processes must occur slowly to keep the gas temperature constant and rapidly without any flow of heat in or out of the system, respectively. In practice, most expansion and compression processes are somewhere in between or said to be polytropic [2]. Examples of an adiabatic process are a piston working in a cylinder and can also be found in astrophysics, nature, and quantum mechanical descriptions of simple atomic systems. A detailed study of the limits of adiabaticity in such slowly varying processes has been recently reported [3].

When a star explodes and becomes a supernova, the time scale of the ejected material can be short compared to the radiative cooling time scale, resulting in a roughly adiabatic expansion. Adiabatic cooling occurs in the terrestrial atmosphere with the formation of clouds as well. For closed systems, the concepts of an adiabatic enclosure and of an adiabatic wall are fundamental. The first law is constructed on the concept of a wall with certain properties: those enclosing arbitrary systems that allow them to remain in their own states of internal thermodynamic equilibrium are defined as adiabatic. Easy to state, but difficult to construct in the real world. In the examples above, which are generally considered adiabatic, a good 40% of the internal energy is lost as heat, somewhere, somehow. The primary culprit is the walls, and where do we draw the boundaries of our little universe?

The expansion of a gas has been understood using traditional thermodynamics. It is convenient to characterize the expansion of a gas using the concept of a polytropic index γ as $PV^{\gamma} = \text{const}$, where γ is equal to unity for the isothermal expansion and to the specific heat ratio γ_a for the adiabatic expansion; i.e., $\gamma = \gamma_a = (N_d + 2)/N_d$, where N_d, the number of degrees of freedom, is 3 for monatomic ($\gamma_a = 5/3$). The polytropic relation can be rewritten using the normalized temperature T/T_0 and density n/n_0 as

$$T/T_0 = (n/n_0)^{\gamma-1}. \tag{1}$$

Whereas experiments with simple gases can be easily carried out in laboratories, those involving gaseous plasmas of astrophysical and solar interest pose a number of extremely difficult problems. Observations near the Sun and at Earth orbit have been interpreted as demonstrating that the solar wind does not expand adiabatically from the Sun as would have been expected for this near collisionless environment. Rather, it expands isothermally, implying that heating of the plasma occurs as it propagates through interplanetary space [4–6]. Many laboratory experiments under adiabatic conditions [7–9] have also shown a nearly isothermal expansion with $\gamma \sim 1.0 - 1.2$ in magnetic nozzles, and the relation with astrophysical plasmas has been discussed [10]. However, in these expanding adiabatic systems, it appears that electric fields may have a significant nonlocal effect on the dynamics of the electrons; many of them are trapped in the system by the ambipolar and wall sheath electric fields, allowing an isothermal equilibrium to

be established after sufficient time has elapsed, while some of the electrons having the energy overcoming the potential drop can escape from the system. Hence, both the trapped and free electrons coexist in different proportions. A very fundamental question then arises: what would happen if there were no electric fields trapping the electrons?

Here, energy distribution of the magnetically expanding electron gas whose charges are neutralized by background ions is measured when removing the electric field from the system. Since the magnetic field can behave as a flexible wall with no physical boundary, it can be considered as a boundary with no heat transfer, i.e., an adiabatic wall. The results demonstrate that the electron gas behaves like an ideal gas expanding adiabatically in the absence of electric fields, while showing isothermal properties when trapped by the electric fields in the system.

The experimental apparatus in Fig. 1(a) is separated into two systems that are electrically isolated from each other by a 2.6-cm-inner-diameter quartz tube: an electron beam source (left) and a grounded diffusion chamber (right) pumped down to a base pressure of 5×10^{-7} Torr. Argon gas of 5 sccm is introduced from the left side of the beam source resulting in a pressure of 0.5 mTorr in the diffusion chamber. A voltage V_D of 200 V is pulsed for 55 msec through a 15 Ω resistor between a hot spiral tungsten filament placed at $z = -25$ cm and an anode mesh at $z = -20$ cm, causing the thermionic electrons from the filament to be accelerated into the quartz tube, producing a high density plasma. The voltage drop across the resistor reduces the accelerating potential to about 100 V. Two solenoids centered at $z = -1.3$ and -15.8 cm provide a uniform magnetic field at the beam source and along the quartz tube before expanding in the diffusion chamber, as seen in Fig. 1(b). The electron Larmor radius is ~4 mm at $z = 30$ cm assuming a temperature of 5 eV; hence, the magnetic field strength is sufficiently high to magnetize the

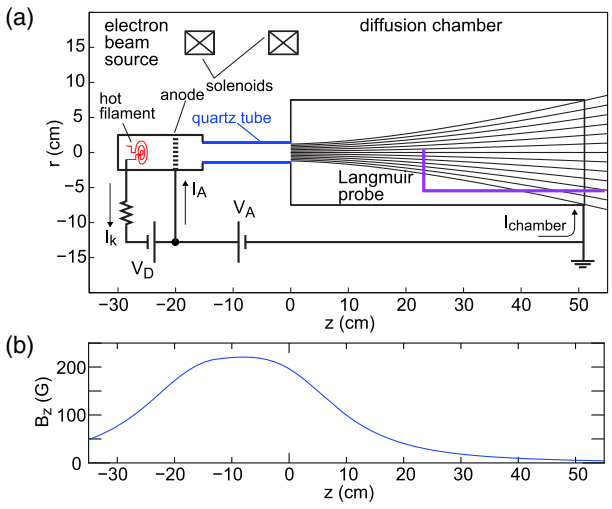

FIG. 1. (a) Schematic of the experimental setup. (b) Axial profile of the magnetic field on axis.

electrons in the chamber. Electrons can be drawn from the source plasma to the right end wall by applying a voltage (V_A) between the beam source and the chamber. The ambipolar and end sheath electric fields are profoundly influenced by changing V_A, as described later.

The electron energy probability functions (EEPFs) are measured using a radially oriented 0.9-mm-diameter and 3-mm-long cylindrical Langmuir probe and an analogue differentiation technique [11]. About 20 msec after the initiation of the plasma pulse, the plasma density has stabilized, allowing the probe bias voltage to be swept for 30 msec. The signals are digitized by a 16-bit data acquisition system and averaged over 100 shots. The electron density n_e and the effective electron temperature T_{eff} can be obtained by integrating the EEPFs as Eq. (10) in Ref. [11]. The plasma potential V_p corresponds to the bias voltage for the zero crossing of the second derivative curve. Since the phase lag of the differentiator causes a small error in the measurement of V_p (typically a few volts), more precise V_p values are obtained from the numerical derivatives of the I-V characteristics.

Figure 2(a) shows the measured axial profiles of V_p for $V_A = 60$ and 0 V. A high plasma potential is maintained for the $V_A = 60$ V case, decreasing about 5 V along the axis. The potential of the end wall ($z = 51$ cm) is shown by a triangle with the dotted lines being visual guides that include the wall sheath. Electrons having an energy less than the ambipolar and sheath potential drops are trapped, as illustrated by the arrow, and an electron current flows toward the anode rather than toward the end wall. A very different scenario is obtained by setting the anode potential $V_A = 0$ V: V_p was measured to be zero along the axis right up to the end wall as shown by the open circles in Fig. 2(a). In this case, there is an electron current away from the anode and electrons from the plasma source freely escape to the end wall. Since a lot of electrons are injected from the source to the diffusion chamber, both the sheath and ambipolar potential drops inhibiting the electron loss are not required to maintain the charge neutrality; hence, the

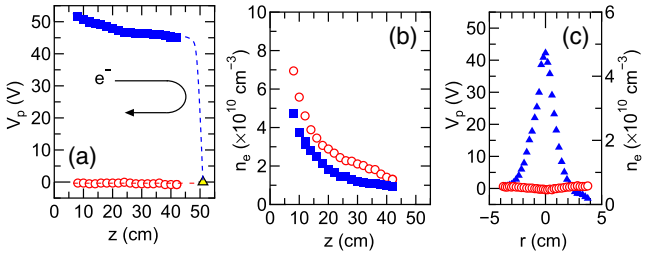

FIG. 2. (a) Axial profile of V_p for $V_A = 60$ V (filled squares) and 0 V (open circles). A triangle shows the grounded wall potential at $z = 51$ cm, the dashed lines being added as visual guides. (b) Axial profile of n_e for the same values of V_A. (c) Radial profile of V_p (open circles) and n_e (filled triangles) taken at $z = 10$ cm for $V_A = 0$ V.

zero plasma potential is formed for the $V_A = 0$ V case. Since there are now no electric fields in the expansion region, there are no electrons returning to the magnetic nozzle throat. Figure 2(b) shows the axial profiles of n_e for both cases; regardless of the presence or not of the axial electric fields, n_e decreases along the axis due to the expansion along the magnetic nozzle. The radial profiles of V_p and n_e for $V_A = 0$ V in Fig. 2(c) show that the radial electric field is completely removed for $V_A = 0$ V, clearly demonstrating that there are no electric fields within the plasma, while maintaining the radial density gradient. For the present electron density and neutral pressure in the chamber, all the collision lengths relating to electrons are longer than the chamber length; i.e., the electrons are collisionless in the diffusion chamber.

Figure 3(a) shows that V_p can be controlled over a wide range by varying V_A. To distinguish between the trapped and free electrons, the typical EEPFs measured at $z =$ 25 cm are shown in Fig. 3(b) for different values of V_A. For the $V_A = 60$ V case, most of the electrons are reflected by the ambipolar and sheath electric fields, and these trapped electrons include the low energy electrons from the source and the remnants from the beam. But as V_p decreases with decreasing V_A, fewer and fewer electrons in the EEPF are reflected until at $V_A = 0$ V when there are no electric fields in the plasma, no electrons are reflected, and all directly escape to the grounded right end wall. The measured electric currents I_{chamber}, I_k, and I_A [labeled in Fig. 1(a)] in Fig. 3(a) show the net flow of electrons to the chamber for the $V_A = 0$ V case, while the negligible electron flow and the ion flow to the chamber are confirmed by the small negative current for $V_A = 60$ V. It is mentioned that the EEPFs in Fig. 3(b) include the hot tail electrons rather than the beam electrons, which is expected to be due to energy scattering via a convective beam-plasma instability and the plasma-wave interaction [12,13]. This Letter focuses on the magnetic nozzle region (diffusion chamber), and measurement of the EEPFs in the source, which would affect the EEPFs entering the chamber, is a subject for further study.

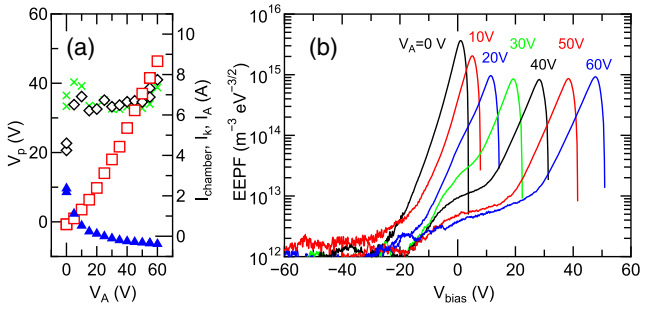

FIG. 3. (a) V_p (open squares) measured at $z = 25$ cm and the electric currents I_{chamber} (filled triangles), I_k (crosses), and I_A (open diamonds). (b) EEPFs plotted versus the probe bias voltage V_{bias}, measured at $z = 25$ cm as a function of V_A.

These EEPFs can be more easily understood if plotted from the viewpoint of an energy frame, meaning that V_p is taken as zero energy. The EEPFs are shown measured along z for the $V_A = 0$ V [Fig. 4(a)] and $V_A = 60$ V [Fig. 4(b)] cases. The same EEPFs plotted over the energy range up to 25 eV are also shown in Figs. 5(a) and 5(b) for clarification of the low energy part and further discussion later. The EEPFs for $V_A = 0$ V show a very rapid decrease of the energetic tail electrons as z is increased, while for $V_A = 60$ V, the energetic electrons exist for all values of z. For the latter case, most of the electrons are reflected by the grounded wall sheath and return to the source; hence, the density of the energetic electrons is much greater than that for the $V_A = 0$ V case.

The n_e and T_{eff} can be obtained by integrating the EEPFs in Figs. 4(a) and 4(b) over the whole energy range in the measurements. By plotting the normalized n_e and T_{eff} in Fig. 4(c), together with the curves calculated using Eq. (1), the polytropic behavior of the electrons can be examined. Electrons in the plasma containing the electric fields are very close to isothermal with $\gamma \sim 1$–1.2 being consistent with the previous measurement of the nonlocal EEPFs [7], as can also be seen from Figs. 4(b) and 5(b), where the slopes of the bulk electrons (hence their temperatures) are comparable for all values of z. It should be noted that the filled squares plotted in upper right of Fig. 4(c) ($T_{\text{eff}}/T_{\text{eff0}} > 0.9$) include a significant contribution from the remnant beam electrons and this strongly affects T_{eff}. The decrease in T_{eff} and increase in γ toward ~1.2 for $T_{\text{eff}}/T_{\text{eff0}} < 0.9$ are due to the decay of the beam electrons. For the case containing no trapped electrons, the slopes of the EEPFs shown in Figs. 4(a) and 5(a) increase with the increase in z, representing a decrease in the temperature of the bulk electrons. Here, the remnant beam electrons are

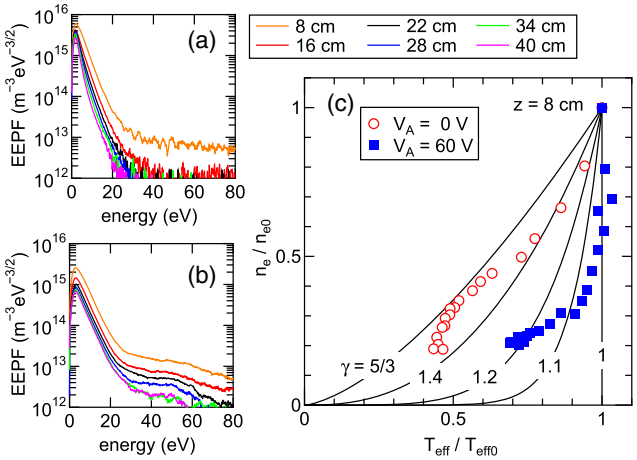

FIG. 4. EEPFs over the range of 0–80 eV as a function of z for (a) $V_A = 0$ V and (b) $V_A = 60$ V. (c) Polytropic relation obtained using the data in Figs. 4(a) and 4(b), together with the calculated curves from Eq. (1) for various values of γ, ranging from isothermal ($\gamma = 1$) to adiabatic expansion ($\gamma = 5/3$).

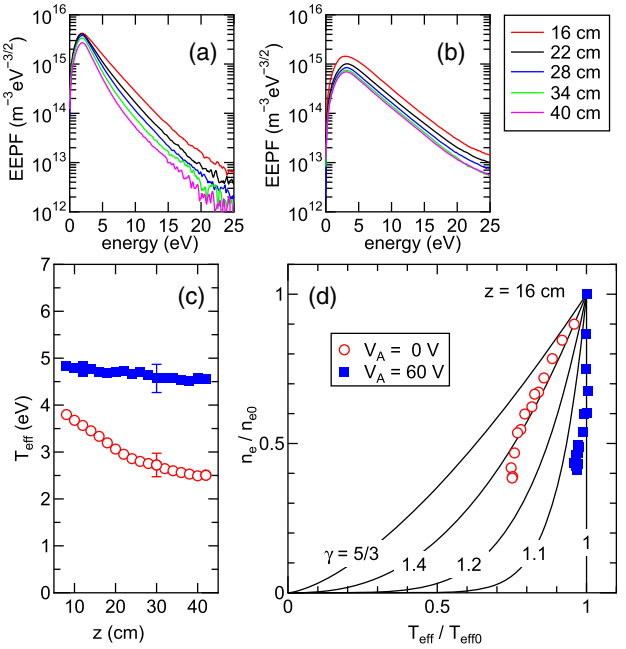

FIG. 5. EEPFs extracted from Fig. 4 data (less than 25 eV and z greater than 15 cm) as a function of z for (a) $V_A = 0$ V and (b) $V_A = 60$ V. (c) T_{eff} obtained by integrating the EEPFs over the energy less than 25 eV for $V_A = 0$ V (open circles) and $V_A = 60$ V (filled squares). (d) Polytropic relation obtained from the data in Figs. 5(a) and 5(b), together with the calculated curves from Eq. (1).

about an order of magnitude less intense compared to the case with the trapped electrons and they play a far less significant role in determining T_{eff}. The polytropic index γ given by the circles in Fig. 4(c) is above 1.4, much larger than that given by the filled squares, and approaches the adiabatic value of $5/3$.

Clearly, the remnant beam components close to the noise level of the measurement affect the derivation of T_{eff}. Consequently, the effective temperatures of the bulk electrons need to be looked at in further detail. There are two particular phenomena that contribute to possible errors in the derivation of T_{eff}: the remnant beam electrons and the magnetic field effects on the Langmuir probe diagnosis. The former was investigated by excluding the tail component and truncating the data by only considering the energy less than 25 eV, yielding the results shown in Fig. 5. The gyroradius has to be larger than the probe tip radius for the present analysis to be valid. The probe tip radius of 0.45 mm corresponds to the Larmor radius of representative low-energy electrons at 1 eV for a magnetic field of 75 G. To minimize these effects, measurements are only considered for z having a magnetic field strength less than about 50 G, which corresponds to $z > 15$ cm.

The slopes of the EEPFs in Fig. 5(a) increase, representing electron cooling, as a function of z, while the slopes in Fig. 5(b) are nearly constant, as mentioned earlier. T_{eff} obtained by integrating the EEPFs over the energy less than 25 eV is plotted in Fig. 5(c), showing a clear decrease of the bulk electron temperature along the axis for the free expansion case ($V_A = 0$ V), as would be expected for an adiabatic expansion, and a constant temperature (isothermal expansion) for the trapped electrons ($V_A = 60$ V). The polytropic relations obtained from the EEPFs in Figs. 5(a) and 5(b) are plotted together with the theoretical curves [Eq. (1)]. This result shows that the electrons are effectively adiabatic for $V_A = 0$ V and isothermal for $V_A = 60$ V. In other words, when the electric field is eliminated from the system, the electrons effectively behave like an adiabatic ideal gas in the magnetic nozzle.

Keeping in mind the first law of thermodynamics, there must be no heat transfer, but work must be done on the walls surrounding the system. Here, the expanding magnetic field can be considered as the wall that has work done on it, but as it is not a physical boundary, no heat is transferred. When the boundary sheath and ambipolar electric fields within the plasma are removed, none of the electrons are trapped in the plasma system and they can only interact with the confining magnetic wall: the plasma pressure force does work on the magnetic boundary.

This can also be understood via the Lorentz force. When the electric field is removed, the force to the electron gas can be given by $\mathbf{J} \times \mathbf{B}$, where the major component of $\mathbf{J}$ is the electron diamagnetic current resulting from the pressure gradient [14]. A force equal in magnitude and opposite in direction to the $\mathbf{J} \times \mathbf{B}$ force is exerted on the magnetic field lines; it is often observed either via the modification of the magnetic field lines [15–17] being considered as the flexible adiabatic wall or directly measured as a thrust force propelling the spacecraft [18]. Hence, the decrease in the electron temperature results from lowering the internal energy of this adiabatic system when the electron gas does work on the expanding magnetic field. This implies that classical thermodynamic principles can be extended to the expansion of a collisionless electron gas in a magnetic nozzle.

The extension of classical thermodynamics for modern physics (non-Gaussian Brownian diffusion in soft-matter [19], microscale engines, and motors [20–22]) out of equilibrium systems (granular gas and materials [23–25], the construction of phase diagrams in hard sphere packing in three dimension [26], and plasma [27]) and open systems is an active emerging field of research. The limit and breakdown of adiabaticity has been analytically and numerically studied in quantum systems [3]; subsequently, possible experimental testing using ultracold gases has been discussed [28,29]. Here, we have removed the effect of plasma boundaries and related electric field on a far-from-equilibrium magnetically expanding electron gas, allowing it to interact solely with the magnetic wall, demonstrating an adiabatic expansion.

The authors would like to thank Professor M. Shats, Dr. N. Francois, and Dr. H. Xia for their useful discussion

of the results. This work is partially supported by a grant-in-aid for scientific research (16H04084 and 26247096) from the Japan Society for the Promotion of Science and Intelligent Cosmos Foundation.

*kazunori@ecei.tohoku.ac.jp

[1] I. H. Hutchinson, *Principles of Plasma Diagnostics*, 2nd ed. (Cambridge University Press, Cambridge, England, 2002).
[2] G. P. Horedt, *Polytropes: Applications in Astrophysics and Related Fields* (Springer, New York, 2004).
[3] A. Polkovnikov and V. Gritsev, Nat. Phys. **4**, 477 (2008).
[4] T. V. Doorsselaere, N. Wardle, G. D. Zanna, K. Jansari, E. Verwichte, and M. Nakariakov, Astrophys. J. Lett. **727**, L32 (2011).
[5] C. Jacobs and S. Poedts, Adv. Space Res. **48**, 1958 (2011).
[6] A. Retinó, Nat. Phys. **12**, 1092 (2016).
[7] Y. Zhang, C. Charles, and R. W. Boswell, Phys. Rev. Lett. **116**, 025001 (2016).
[8] J. M. Little and E. Y. Choueiri, Phys. Rev. Lett. **117**, 225003 (2016).
[9] J. P. Sheehan, B. W. Longmier, E. A. Bering, C. S. Olsen, J. P. Squire, M. G. Ballenger, M. D. Carter, F. R. Chang Díaz, T. W. Glover, and A. V. Ilin, Plasma Sources Sci. Technol. **23**, 045014 (2014).
[10] Y. Zhang, C. Charles, and R. W. Boswell, Astrophys. J. **829**, 10 (2016).
[11] K. Takahashi, C. Charles, R. W. Boswell, and T. Fujiwara, Phys. Rev. Lett. **107**, 035002 (2011).
[12] C. T. Dum and R. N. Sudan, Phys. Fluids **14**, 414 (1971).
[13] R. W. Boswell, S. M. Hamberger, P. J. Kellogg, I. Morey, and R. K. Porteous, Phys. Lett. **101A**, 501 (1984).
[14] K. Takahashi, C. Charles, and R. W. Boswell, Phys. Rev. Lett. **110**, 195003 (2013).
[15] C. S. Corr and R. W. Boswell, Phys. Plasmas **14**, 122503 (2007).
[16] B. R. Roberson, R. Winglee, and J. Prager, Phys. Plasmas **18**, 053505 (2011).
[17] K. Takahashi and A. Ando, Phys. Rev. Lett. **118**, 225002 (2017).
[18] K. Takahashi, T. Lafleur, C. Charles, P. Alexander, and R. W. Boswell, Phys. Rev. Lett. **107**, 235001 (2011).
[19] B. Wang, J. Kuo, S. C. Bae, and S. Granick, Nat. Mater. **11**, 481 (2012).
[20] V. Blickle and C. Bechinger, Nat. Phys. **8**, 143 (2012).
[21] S. Krishnamurthy, S. Ghosh, D. Chatterji, R. Ganapathy, and A. K. Sood, Nat. Phys. **12**, 1134 (2016).
[22] I. A. Martínez, A. Petrosyan, D. Guéry-Odelin, E. Trizac, and S. Ciliberto, Nat. Phys. **12**, 843 (2016).
[23] F. Rouyer and N. Menon, Phys. Rev. Lett. **85**, 3676 (2000).
[24] J. S. van Zon and F. C. MacKintosh, Phys. Rev. Lett. **93**, 038001 (2004).
[25] M. Saadatfar, H. Takeuchi, V. Robins, N. Francois, and Y. Hiraoka, Nat. Commun. **8**, 15082 (2017).
[26] C. Song, P. Wang, and H. A. Makse, Nature (London) **453**, 629 (2008).
[27] B. Liu and J. Goree, Phys. Rev. Lett. **100**, 055003 (2008).
[28] J. Tuoriniemi, Nat. Phys. **12**, 11 (2016).
[29] W. Zwerger, Nat. Phys. **4**, 444 (2008).